

Article

On-Site Investigations of Coastal Erosion and Accretion for the Northeast of Taiwan

Ting-Yu Liang ¹, Chih-Hsin Chang ¹, Shih-Chun Hsiao ² , Wei-Po Huang ³ , Tzu-Yin Chang ¹, Wen-Dar Guo ¹, Che-Hsin Liu ¹, Jui-Yi Ho ¹  and Wei-Bo Chen ^{1,*} 

- ¹ National Science and Technology Center for Disaster Reduction, New Taipei City 23143, Taiwan; lty@ncdr.nat.gov.tw (T.-Y.L.); chang.c.h@ncdr.nat.gov.tw (C.-H.C.); geoct@ncdr.nat.gov.tw (T.-Y.C.); wdguo@ncdr.nat.gov.tw (W.-D.G.); a120160@ncdr.nat.gov.tw (C.-H.L.); juiyiho@ncdr.nat.gov.tw (J.-Y.H.)
- ² Department of Hydraulic and Ocean Engineering, National Cheng Kung University, Tainan City 70101, Taiwan; schsiao@mail.ncku.edu.tw
- ³ Department of Harbor and River Engineering, National Taiwan Ocean University, Keelung City 202301, Taiwan; a0301@mail.ntou.edu.tw
- * Correspondence: wbchen@ncdr.nat.gov.tw; Tel.: +886-2-8195-8611

Abstract: Coastal erosion is a major natural hazard along the northeastern shoreline (i.e., Yilan County) of Taiwan. Analyses of the evolution of the 0 m isobath of the Yilan County coastline indicate that erosion and accretion are occurring north and south of Wushi Fishery Port, respectively, because of jetty and groin construction. Topographic and bathymetric surveys involving the measurement of 43 cross sections were conducted in 2006, 2012, 2013, and 2019. The cross-shore profile comparisons reveal that the erosion of onshore dunes is significant in the northern Jhuan River estuary. Due to the establishment of a nature reserve in the southern Lanyang River estuary, the sediments are carried northward by tidal currents, and accretion is inevitable in the northern Lanyang River estuary. The results of the bathymetric surveys also suggest that the shoreline of Yilan County tends to accrete in summer because of abundant sediment from the rivers; however, it is eroded in winter, owing to the large waves induced by the northeast monsoon. Additionally, the calculated net volume of erosion and accretion between each pair of cross sections shows that the length of coastline impacted by estuarine sediment transport is approximately 2 km long from north to south along the coastline of the Lanyang River estuary.

Keywords: erosion and accretion; cross-shore profile evolution; Lanyang River estuary; limit of estuarine sediment transport; northeastern coastal waters of Taiwan



Citation: Liang, T.-Y.; Chang, C.-H.; Hsiao, S.-C.; Huang, W.-P.; Chang, T.-Y.; Guo, W.-D.; Liu, C.-H.; Ho, J.-Y.; Chen, W.-B. On-Site Investigations of Coastal Erosion and Accretion for the Northeast of Taiwan. *J. Mar. Sci. Eng.* **2022**, *10*, 282. <https://doi.org/10.3390/jmse10020282>

Academic Editor: Rodger Tomlinson

Received: 7 February 2022

Accepted: 10 February 2022

Published: 18 February 2022

Publisher's Note: MDPI stays neutral with regard to jurisdictional claims in published maps and institutional affiliations.



Copyright: © 2022 by the authors. Licensee MDPI, Basel, Switzerland. This article is an open access article distributed under the terms and conditions of the Creative Commons Attribution (CC BY) license (<https://creativecommons.org/licenses/by/4.0/>).

1. Introduction

Coastal erosion can lead to coastal retreat, habitat destruction, and loss of land, which result in significant negative ecological and socioeconomic impacts on global coastal zones. Beach and dune systems are the first line for defending against the damaging impacts of water-related natural hazards, such as coastal storms, hurricanes, and typhoons; therefore, shoreline erosion (retreat) poses a significant threat to settled coastal areas worldwide [1,2]. Rapidly changing coastlines are a serious problem in many areas of the world, such as sections of the Nile and the Yellow River Delta, which have stirred the interest of many researchers in different fields [3–20].

The sediment budget and geology determine coastal morphology and dynamics, which influence the nature and health of coastal ecosystems. Human activities affecting sediment dynamics, both on the coast and on land, modify the naturally occurring patterns of erosion and accretion. Additionally, human interventions have frequently altered the delivery of riverine sediments to coastal areas [21–24]. For example, reservoir/dam construction has trapped over 50% of the world's sediment flux [25], and most of the world's deltas have now been significantly dammed in their upper and central reaches [21,25].

According to the report from Warrick et al. [26], approximately 30 million tons (Mt) of sediment was deposited in the reservoirs of the river they studied before dam removal began in 2011.

Many areas of observed historical shoreline advances are related to reclamation and impoundment by coastal structures. These human activities modify coastal dynamics, typically resulting in downdrift erosion. Factors that influence coastal erosion and sedimentation encompass characteristics of coastal sediment; exchanges among the land, the coast, and the shelf; geomorphic responses to oceanic forcing. Human activities may both substantially influence and be affected by coastal erosion and sedimentation [2,27,28]. Currently, climate change impacts, including sea-level rise and potential increases in the frequency and intensity of severe tropical and extratropical storms, hurricanes, and typhoons, could accelerate coastal erosion or accretion, and recent observations have also indicated an acceleration in coastal cliff erosion [29].

Dadson et al. [30] reported erosion rates in the Taiwan Mountains estimated from modern river sediment loads. They suggested that Taiwan supplied 384 Mt yr^{-1} of suspended sediment to the ocean from 1970 to 1999, which represents 1.9% of the estimated global suspended sediment discharge but is derived from only 0.024% of Earth's subaerial surface. A better understanding of the nature and evolution of coastal (beach) erosion and accretion is necessary to inform and enact appropriate and timely disaster preparedness [31,32]. Moreover, to accurately assess coastal hazards in the face of future climate and land-use changes, it is necessary to understand the dynamics of shoreline erosion and accretion over the length and time scales relevant to the processes that drive change.

Direct measurements through traditional on-boat acoustic surveys have a high resolution, although they consume considerable manpower and material resources [33]. The present study investigated the timing of the transition from either stable or erosional conditions to accretional conditions in the study area by evaluating a time series of cross-shore positions. The aim and insights derived from the present study are expected to clarify coastal, beach, estuarine, and tidal flat management strategies. The findings are also helpful for the development of similar coastal systems worldwide. The details of the study site information, the evolution of the 0 m isobath, on-site topography, and bathymetric survey are described in Section 2; the analyses of interannual and seasonal variability derived from the surveyed data are presented in Section 3. In Section 4, a discussion on the alongshore limit of the sediment delivered from the Lanyang River is given, and finally, the summary and conclusions are presented in Section 5.

2. Materials and Methods

2.1. Description of Study Site

Yilan County covers the entire shoreline of northeastern Taiwan, with a total length of 101 km. The whole coastline is categorized as a fault coast in northern and southern Yilan and an alluvial-plain coast in middle Yilan according to the geological features. The section of shoreline selected for topographic and bathymetric surveys extended from north of the Wushi Fishery Port to south of the Lanyang River estuary, with a length of nearly 20 km (red line in Figure 1a), and extended from the shoreline to approximately 800 to 1000 m offshore. Figure 1b shows an aerial image of the Wushi Fishery Port taken in the present study. As shown in Figure 1b, an offshore jetty and an extended jetty, with lengths of 500 m and 400 m, respectively, lie to the east and north of the Wushi Fishery Port, respectively, to stabilize the oscillation caused by waves. A wave buoy located west of Gueishan Island (the orange triangle in Figure 1a) is managed by the Central Weather Bureau (CWB) of Taiwan. The hourly measurements of significant wave height and current recorded at the buoy from 2006 to 2020 are graphed in Figure 1c,d, respectively. It is obvious that the predominant waves come from the northeast with a height of 1–2 m (Figure 1c); however, this coastal area is threatened with big waves (significant wave height > 3.0 m) during the passage of typhoons [34,35]. The principal currents range from 0.25 to 0.5 m/s, with a flow direction to the southeast (Figure 1d). Erosion and accretion phenomena are expected to be found in the

north and south of Wushi Fishery Port, respectively, due to the physical characteristics of the marine environment and jetty effect. According to the report from the Water Resource Agency (WRA) of Taiwan, the Lanyang River is the largest river (with a watershed area of 978 km²) in Yilan County and has an average annual runoff of 74.24 ms⁻¹ and a sediment yield of 6 million m³. An aerial image (taken by the present study) of the Lanyang River estuary is shown in Figure 1e, and a sandbar in the south of the Lanyang River estuary is clearly shown. Additionally, the daily sediment emissions from the Lanyang River estuary were measured by the WRA on the specified days in 2020. Figure 2 illustrates the daily variations of estuarine sediment volume at the Lanyang River. It can be seen that the months with higher daily sediment volume in the Lanyang River estuary are the end of April to September each year, due to their being wet and typhoon seasons. The median particle diameter (D50) of the Lanyang River estuary is 5.949 mm, according to the report from the WRA.

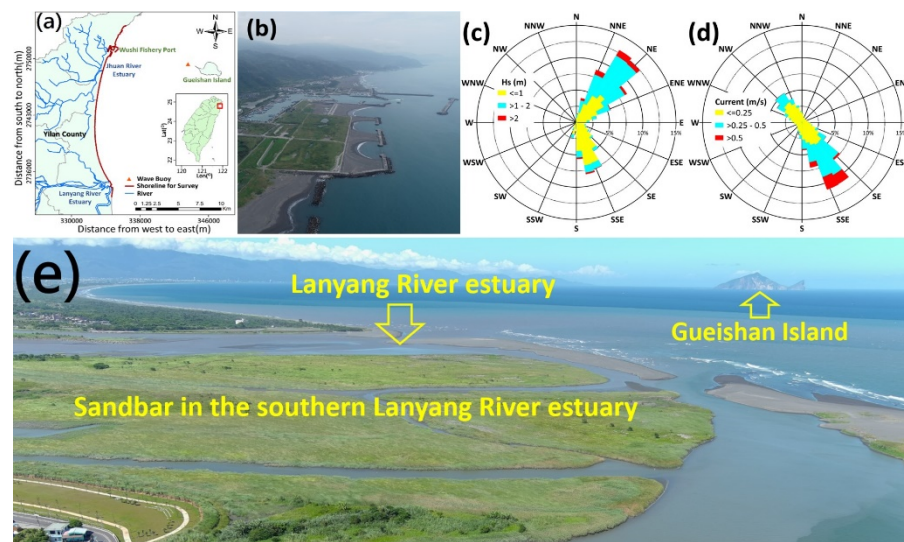


Figure 1. (a) The location of the study area, (b) an aerial image of the Wushi Fishery Port, (c) directional distribution of significant wave height, (d) directional distribution of current measured at a wave buoy near Guishan Island from 2006 to 2020, and (e) an aerial image of the Lanyang River estuary.

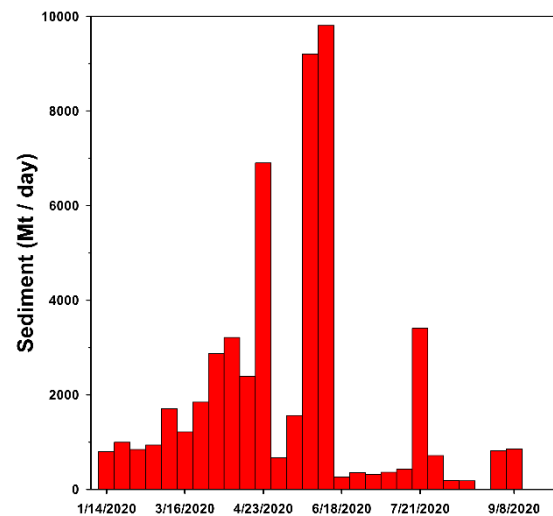


Figure 2. Measurements of daily sediment discharged from the Lanyang River estuary in 2020.

2.2. Evolution of the 0 m Isobath

To better understand the shoreline evolution in the coastal area with significant erosion and accretion phenomena, the 0 m isobaths for the northern and southern Wushi Fishery Port and for the Lanyang River estuary surveyed in 2006, 2013, 2013, and 2019 were collected and compared. Figure 3a,b illustrate the 0 m isobaths along the northern and southern Wushi Fishery Port, respectively, and the 0 m isobath for the Lanyang River estuary is depicted in Figure 3c. As shown in Figure 3a, the 0 m isobath extended offshore to the north of the Wushi Fishery Port by 2013 due to the construction of the jetty and groin. The 0 m isobath in the southern Wushi Fishery Port stretched offshore and reached its maximum in 2013, after which erosion occurred until 2015 (as shown in Figure 3b). The 0 m isobaths crossing the Lanyang River estuary in various years are shown in Figure 3c. The 0 m isobaths around the Lanyang River estuary trended offshore by 2012 because of abundant sediments supplied by the Lanyang River; however, they retreated landward until 2015 as a result of the river mouth moving northward and reduced sediment transport southward.

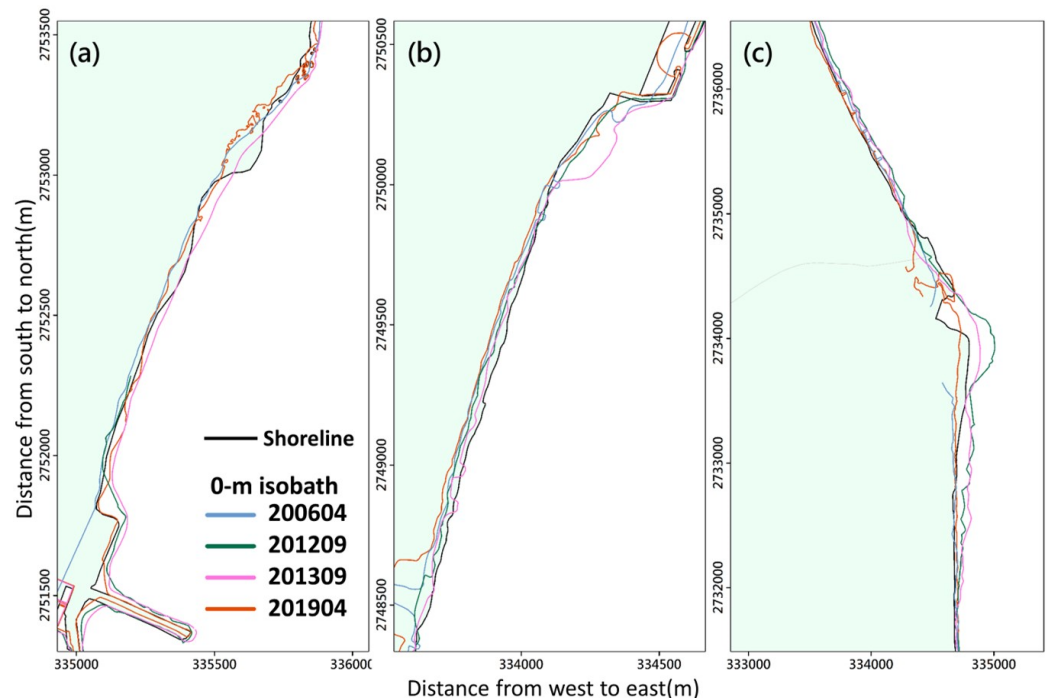


Figure 3. Evolution of the 0 m isobath along (a) the northern Wushi Fishery Port, (b) the southern Wushi Fishery Port, and (c) the Lanyang River estuary.

2.3. On-Site Bathymetric and Topographic Surveys

Multiple methods can be used for bathymetric surveys, e.g., multibeam and single-beam surveys. An accurate bathymetric survey allows the researcher to measure the depth of a water body and map the underwater features of a water body. To analyze the long-term erosion and accretion in the study area, topographic and bathymetric surveys were conducted through the measurement of 43 cross sections along the coastline from north of the Wushi Fishery Port to the south of the Lanyang River estuary in June 2006, April and September 2012, April and September 2013, and April and October 2019. Figure 4 demonstrates the spatial distribution of the cross sections for sampling bathymetry and topography. As shown in Figure 3, the planned survey track lines for the sonar collection were spaced approximately 500 m apart in the alongshore direction and were of varying length to allow the survey to be completed in 2 days. The bathymetric survey was performed offshore from north of the Wushi Fishery Port to the south of the Lanyang River estuary, utilizing a boat-mounted Global Positioning System (GPS) device, with a

single-beam echosounder. The boat bathymetric survey was carried out until the measured water depth was approximately 10–15 m. This is based on the empirical formula proposed by Houston [36], i.e., $hc = 6.75 H_{sm}$, where hc is the closure depth (a water depth of the survey endpoint in nearshore waters) and H_{sm} is the long-term averaged significant wave height, which represents the wave climate of the study area. An H_{sm} value of 1.14 m was adopted in the present study, according to the statistical data for waves issued by the CWB of Taiwan. The hc value is estimated to be approximately 7.7 m for the nearshore waters of Yilan using Houston's equation. In order to avoid the inaccuracy of the depth sounder, the present study extended hc to 10–15 m to ensure the minimal hc (i.e., 7.7 m) is within the bathymetric surveys. A surveying-quality GPS unit and an electronic distance measurement (EDM) total station theodolite (TST) were used to determine the locations of features shown in the present study, to conduct a topographic survey on the beach.

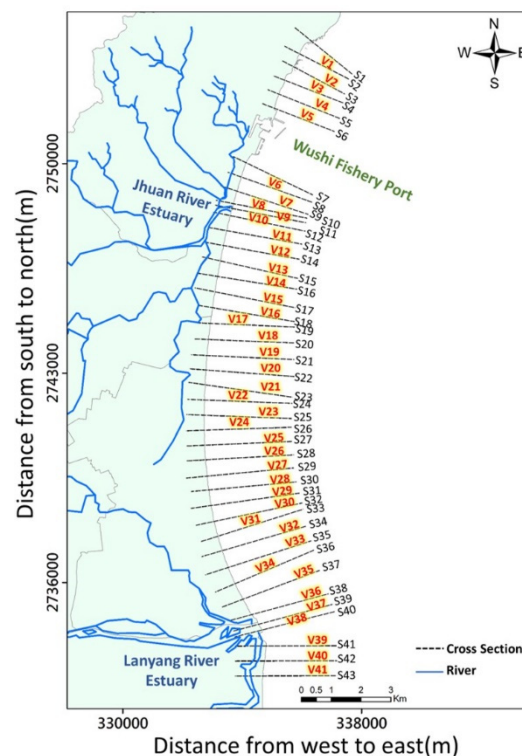


Figure 4. Spatial distribution of the cross sections for sampling bathymetry.

3. Results

3.1. Interannual Variability of Erosion and Accretion along the Surveyed Shoreline

To analyze the long-term variation in erosion and accretion for the study coastline, bathymetric surveys were conducted in June 2006, April and September 2012, April and September 2013, and April and October 2019. A total of 43 transects (track lines) were distributed along the shoreline from north of the Wushi Fishery Port to the south of the Lanyang River estuary (as shown in Figure 4). Moreover, the net volume of erosion or accretion between two transects was estimated, which means that 41 net volumes were used to evaluate whether the sediment budget was increasing or decreasing along the studied coast. The updated bathymetric datasets were compared with the previous datasets to estimate depth changes during two periods. Figure 5a,b present the variations in bottom elevation over 7 and 6 years, respectively, with Figure 5a showing the changes between June 2006 and April 2013 and Figure 5b showing the changes between April 2013 and April 2019.

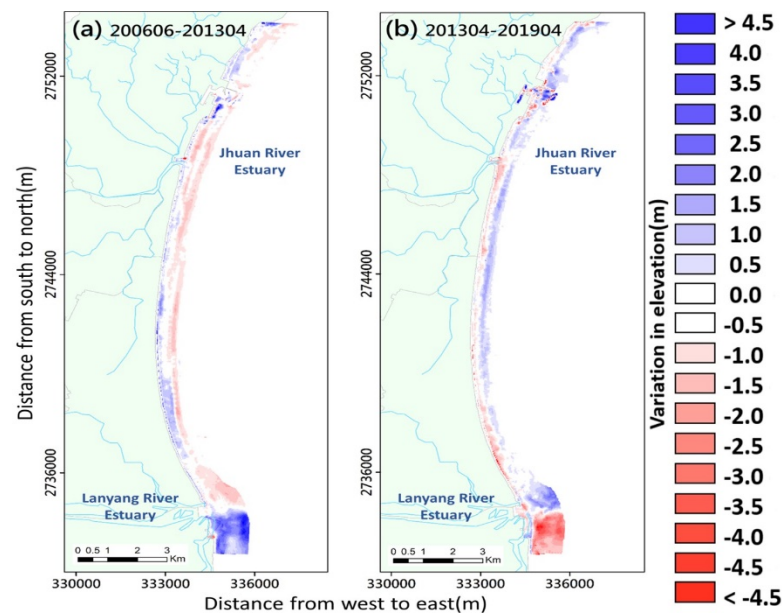


Figure 5. The spatial distribution of erosion and accretion along the shoreline during the periods of (a) June 2006 to April 2013 and (b) April 2013 to April 2019.

The comparisons indicate that erosion and accretion phenomena occurred alternately along the shoreline from north of the Wushi Fishery Port to the south of the Lanyang River estuary and from June 2006 to April 2013 and April 2013 to April 2019. This is particularly obvious in the waters near the Lanyang River estuary. As shown in Figure 5a, the bathymetries rose to a maximum of 3.0–4.0 m in the south of the Lanyang River estuary from June 2006 to April 2013; however, the water depths were reduced by 3.0–4.0 m in the same area from April 2013 to April 2019 (Figure 5b). Overall, the erosion and accretion trends for the waters close to the shoreline are found to be contrary to those of the water slightly farther from the shoreline for both periods. A similar phenomenon is discovered when Figure 5a is compared to Figure 5b. Slight erosion and accretion were distributed in the area somewhat far from the shoreline and the area close to the shoreline, respectively, along the coastline from north of the Wushi Fishery Port to the northern Lanyang River estuary during the period of June 2006 to April 2013 (i.e., a 7-year bottom elevation difference, as shown in Figure 5a). However, the opposite phenomenon of erosion and accretion occurred for the 6-year bottom elevation difference from April 2013 to April 2019 (Figure 5a). Figure 6a,b present the net erosion (positive quantity in Figure 6) or accretion (negative quantity in Figure 6) volume of each pair of transects in the 7-year and 6-year periods, respectively. Based on a comparison of Figure 5 with Figure 6, the distribution pattern of increases and decreases in the net volume is identical to that of the bathymetric changes alongshore. The maximal accretion volumes are approximately $2 \times 10^6 \text{ m}^3$ at two intervals between transects S40 and S41 and between S41 and S42 (i.e., V39 and V40, as shown in Figure 6a), while the maximal erosion volume is nearly $-2 \times 10^6 \text{ m}^3$ at an interval between transects S41 and S42 (i.e., V40, as shown in Figure 6b). To evaluate the longer-term erosion and accretion along the studied shoreline, the differences between the bathymetric surveys in June 2006 and April 2019 were calculated. The variations in bottom elevation and net volume are depicted in Figure 6a,b, respectively. The 13-year alongshore erosion and accretion variations are minor relative to the 7-year and 6-year evolution. The changes in water depth are within $\pm 2.0 \text{ m}$ (as shown in Figure 7a), and the maximum accretion and erosion volumes are approximately $1.0 \times 10^6 \text{ m}^3$ and $-5.0 \times 10^5 \text{ m}^3$ at V39 and V35, respectively (Figure 7b). This means that the sediment added to and removed from the studied coastal system is gradually balanced through long-term sediment transport.

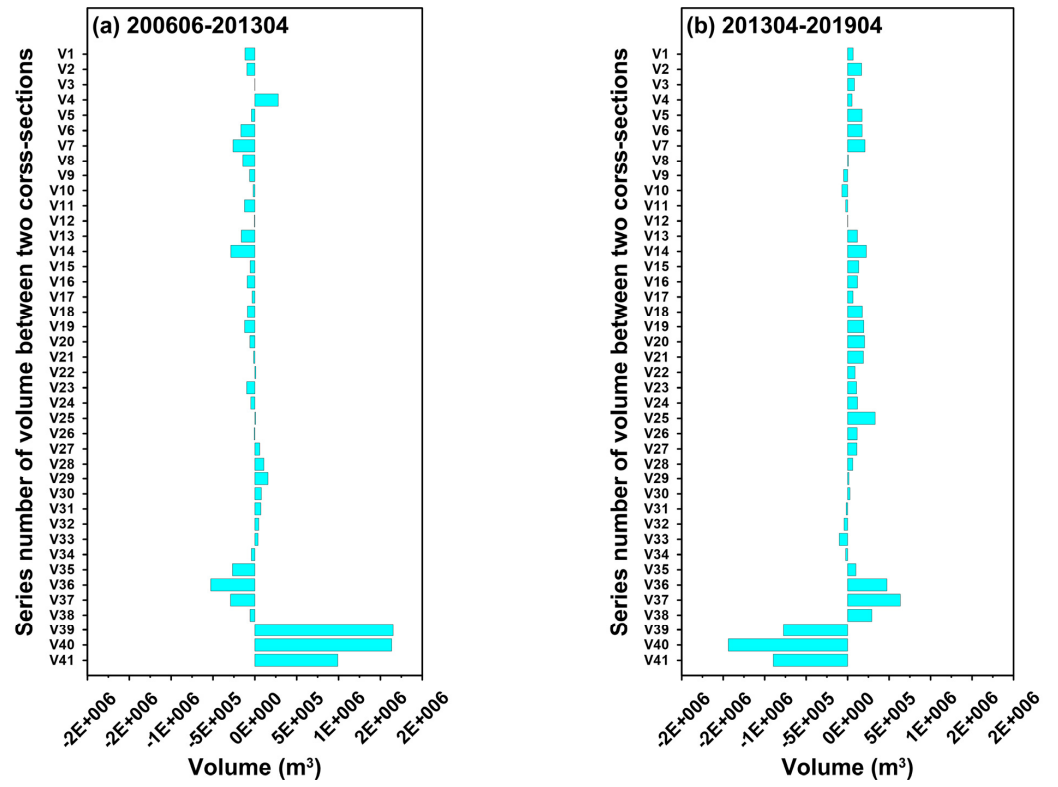


Figure 6. The erosion and accretion volume between each pair of cross sections during the period of (a) June 2006 to April 2013 and (b) April 2013 to April 2019.

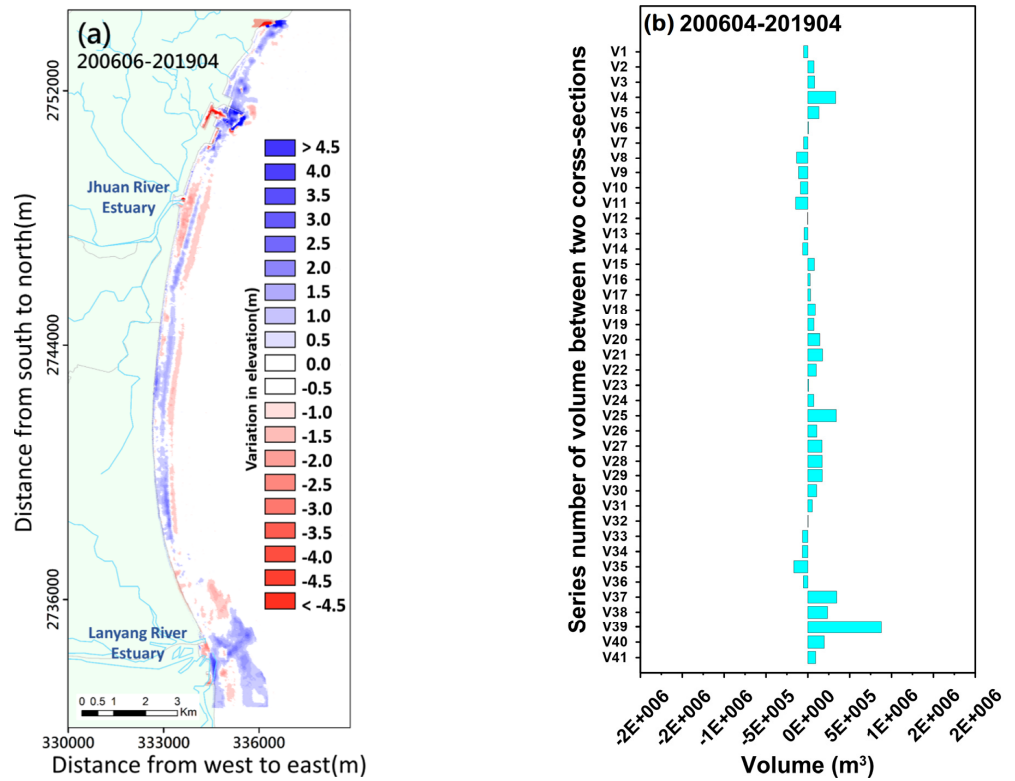


Figure 7. The erosion and accretion volume between each pair of cross sections during the period of (a) June 2006 to April 2013 and (b) April 2013 to April 2019.

3.2. Seasonal Variability in Erosion and Accretion along the Surveyed Shoreline

In addition to the interannual variability in erosion and accretion, estimating the seasonal variation in erosion and accretion is also important to coastal management and development. The bathymetric data pairs surveyed in September 2012 and April 2013 and in April 2013 and October 2013 were adopted to analyze the variability in erosion and accretion along the studied coastline in winter and summer, respectively. The bathymetry differences between September 2012 and April 2013 are regarded as erosion and accretion variations in winter (as shown in Figure 8a), while the bathymetry differences between April 2013 and October 2013 are considered to be erosion and accretion variations in summer (as shown in Figure 8b). As shown in Figure 8a, erosion phenomena are obvious along the shoreline from north of the Wushi Fishery Port to the south of the Lanyang River estuary during winter, due to the sustained large waves caused by the northeast monsoon and the shortage of sediment discharged from the river. In contrast, in summer, accretion phenomena are found along the coastline from north of the Wushi Fishery Port to the Lanyang River estuary (Figure 8b) because of weaker waves and abundant sediment released from the river.

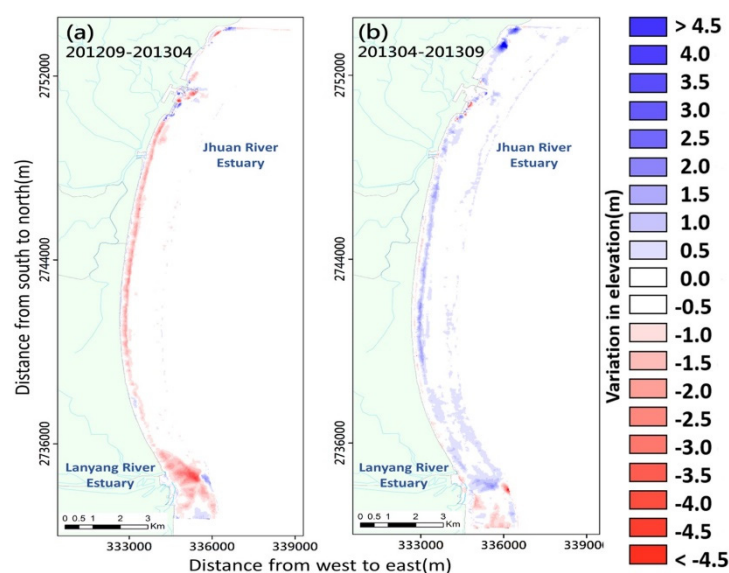


Figure 8. The spatial distribution of seasonal variability for erosion and accretion along the shoreline for (a) winter (from September 2012 to April 2013) and (b) summer (from April 2013 to September 2013).

3.3. Analysis of Cross-Shore Profile Evolution

Eight representative transects illustrated in Figure 9 were selected for cross-profile comparisons with the bathymetric surveys in June 2006, April 2012, April 2013, and April 2019. Cross-profile comparisons are beneficial for investigating nearshore morphological evolution and sediment transport mechanisms in coastal environments. Closure depth has been widely used within coastal engineering as an empirical measure of the seaward limit of significant cross-shore sediment transport on sandy beaches. Therefore, a closure depth of approximately 10 m was adopted as an offshore boundary for morphodynamics in the present study. The cross-profile surveys extended from dune ridges on the beach to the 10 m closure depth in the nearshore waters of the study site. Eight transects were measured in the northern and southern portions of the Wushi Fishery Port (transects S5 and S9 in Figure 9), in the northern and southern portions of the Jhuan River estuary (transects S10 and S11 in Figure 9), along the shoreline between the Jhuan River estuary and the Lanyang River estuary (transects S18 and S31 in Figure 9), and in the northern and southern portions of the Lanyang River estuary (transects S38 and S41 in Figure 9). Figure 10a–d represent the topographic and bathymetric data for transects S5 (Figure 10a), S9 (Figure 10b), S10

(Figure 10c), and S12 (Figure 10d). These transects were surveyed in June 2006, April 2012, April 2013, and April 2019. The cross-profile comparisons of transects S5 and S9 (surveyed in the northern and southern portions of the Wushi Fishery Port) in various years are shown in Figure 10a,c. The bathymetric surveys were all performed after the construction of the Wushi Fishery Port in 2002. The comparisons show that the accretion is sustainable in the northern portion of the Wushi Fishery Port (transect S5) and is up to 2 m at a distance of approximately 400 m from 2006 to 2019 (Figure 10a). Erosion phenomena were found in the southern portion of the Wushi Fishery Port (transect S9) at a distance of 100–400 m; however, weak accretion was detected at a distance of 600–800 m (Figure 10b). The construction of the Wushi Fishery Port, which created a jetty effect, is the major contributing factor to accretion and erosion on the northern and southern sides of the Wushi Fishery Port. The bathymetry changes are minor below a water depth below 0 m on the northern and southern sides of the Jhuan River estuary (transect S10 in Figure 10c and transect S12 in Figure 10d). However, a coastal dune with a height of approximately 7 m in transect S10 (northern side of the Jhuan River estuary) was eroded significantly within a distance of 150 m because of the strong northeast monsoon (Figure 10c). Transects S18 and S31 lay between the Jhuan River estuary and the Lanyang River estuary and feature a gently sloping seafloor (as shown in Figure 11a,b). The cross-profile comparisons are relatively stable because they are far from the estuaries and any artificial structures. Figure 11c,d illustrate the bathymetric variations along transects S38 and S41, respectively, in various years. As shown in Figure 11c (transect S38), erosion occurred in the north of the Lanyang River estuary with a distance between 700 m and 1300 m from 2006 to 2013, after which accretion was present in the same zone. The most significant erosion and accretion are observed in the southern Lanyang River estuary, i.e., transect S41 in Figure 11d. The accretion reached 2–4 m along all of transect S41 from 2006 to 2013, but the coastal and nearshore zones at distances beyond 200 m were eroded dramatically in 2019. These phenomena are identical to the evolution of the 0 m isobath in various years described in Section 2.2. The Lanyang River mouth moved northward gradually, and the supply of riverine sediment for the southern Lanyang River estuary has consequently decreased in the past two decades.

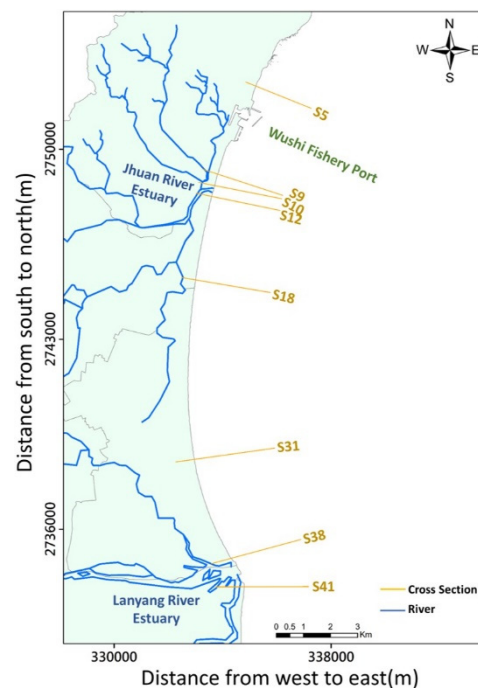


Figure 9. Spatial distribution of eight transects for the cross-shore profile comparison.

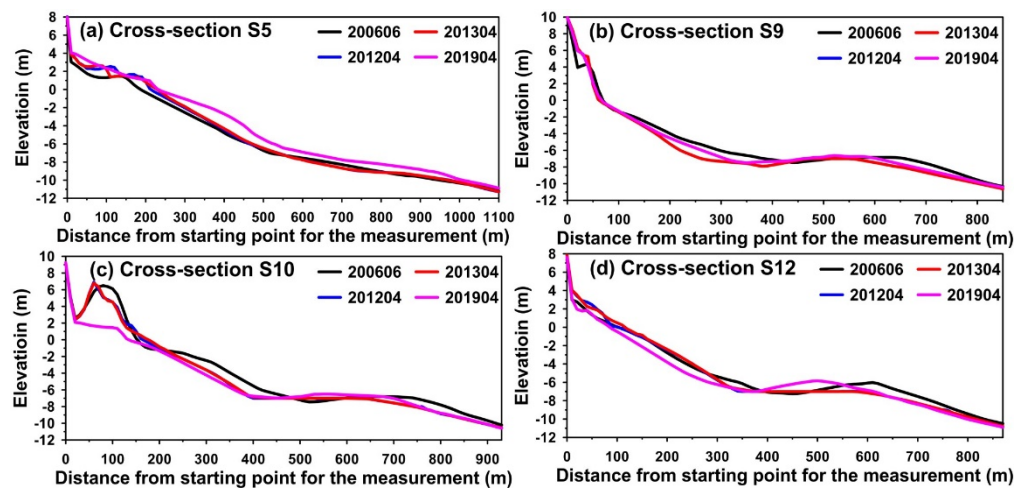


Figure 10. Cross-shore bathymetry profile comparisons for (a) S5, (b) S9, (c) S10, and (d) S12 cross-sections measured in various years.

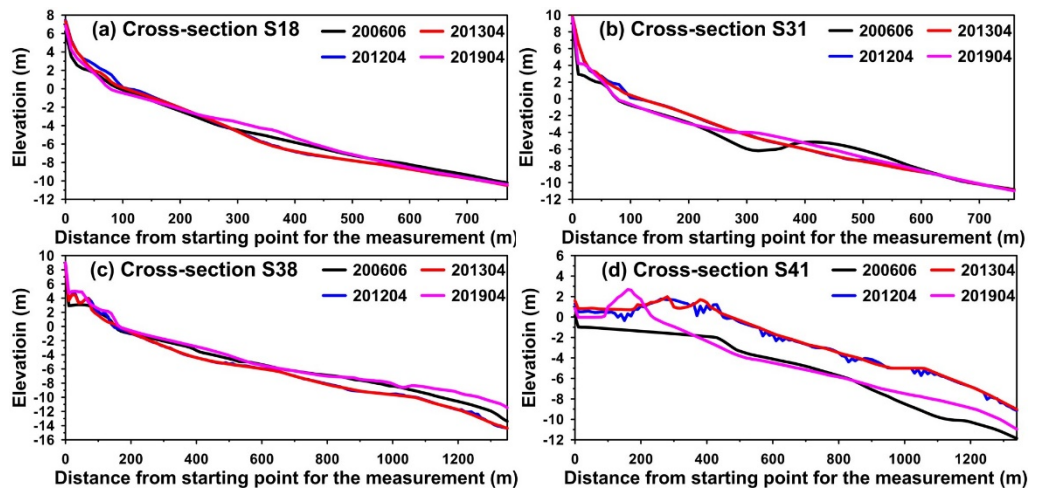


Figure 11. Cross-shore bathymetry profile comparisons for (a) S18, (b) S31, (c) S38, and (d) S41 cross-sections measured in various years.

4. Discussion

According to the evolution of the 0 m isobath and the cross-sectional bathymetric data surveyed in various years, the present study reveals that a drastic morphodynamic pattern is found around the Lanyang River estuary and is particularly obvious in the southern Lanyang River estuary. The topographic and bathymetric data of transects S30–S43 surveyed in June 2006, April 2013, and April 2019 were utilized to clarify the mechanism of estuarine sediment transport for the Lanyang River. The spatial distributions of transects S30–S43 and their corresponding serial numbers for the net volume variation (i.e., V29–S43) are delineated in Figure 12a for June 2006 to April 2013 and in Figure 12b for April 2013 to April 2019. A comparison of Figure 12a,b shows that the erosion and accretion phenomena in the northern Lanyang River estuary are contrary to those in the southern Lanyang River estuary for the two periods. This is because a nature reserve in the southern Lanyang River estuary cannot be developed from 2013. Although the 13-year (June 2006 to April 2019) variations still show a slight accretion in the south of the Lanyang River estuary (Figure 7), erosion began in 2013. The erosion and accretion along the shoreline near the Lanyang River estuary are highly dependent on the estuarine sediment discharge and transport of the Lanyang River. Therefore, the limit of estuarine sediment transport is considered to play an important role in the mechanism of coastal erosion and accretion and can be used to examine how far estuarine sediment can be supplied. The net volume

variations along the coastline of the Lanyang River estuary for the periods from June 2006 to April 2013 (cyan bar) and from April 2013 to April 2019 (red bar) are presented in Figure 12. As shown in Figure 13, erosion and accretion began to reverse at V34 and V38 between the two periods. The accretion turned into erosion from V34 to V38 and then returned to accretion at V39 during the 7-year period (from June 2006 to April 2013, cyan bar in Figure 13). A contrary phenomenon appeared in the same interval (between V34 and V38) in the 6-year period (from April 2013 to April 2019, red bar in Figure 13); in other words, accretion occurred within V34 to V38, but erosion occurred outside this interval. Therefore, it is believed that the extent affected by estuarine sediment is approximately 2 km long from north to south along the coast of the Lanyang River estuary.

Infrastructure and human activity, such as establishing nature reserves and constructing jetties along the coast, modify many of the shorelines worldwide and drive change in coastal geomorphology. These artificial modifications resulted in impairment to the balance of the erosion and accretion in the estuarine and coastal environment. The on-site data surveyed in the present study provides insightful and valuable suggestions in scientific perspectives and coastal zone management.

The extensive set of observed data in the present study are undoubtedly helpful for future comparisons with the results from numerical models to determine the beach shoreline evolution [37,38]; in fact, monitoring activities significantly contribute to improving the robustness and reliability of numerical models [39,40].

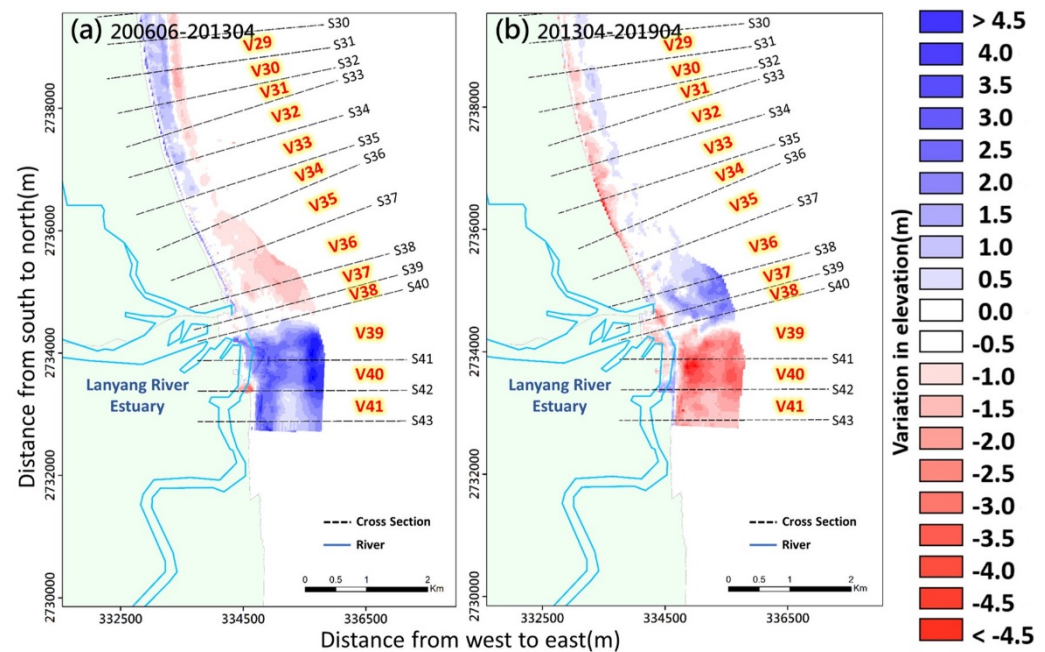


Figure 12. Long-term erosion and accretion and spatial distribution of the cross sections for sampling bathymetry near the Lanyang River estuary during the period of (a) June 2006 to April 2013 and (b) April 2013 to April 2019.

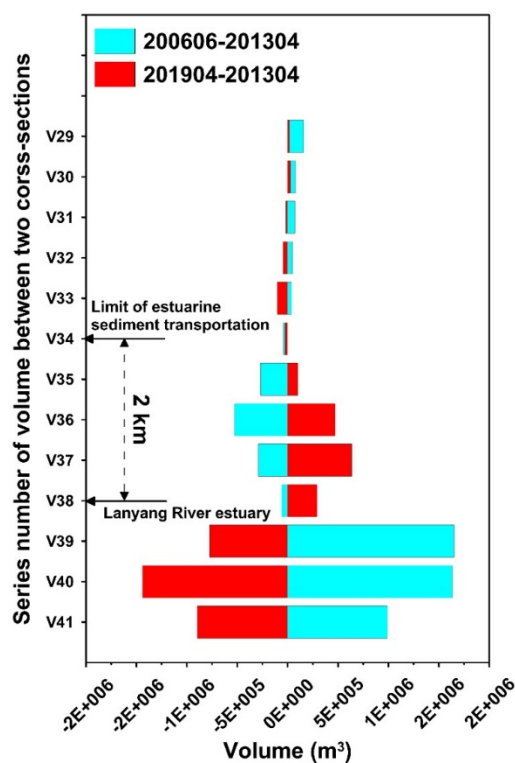


Figure 13. Net volume variations between erosion and accretion around the Lanyang River estuary (corresponding to V29 to V41 in Figure 11) during the period of June 2006 to April 2013 (cyan bar) and April 2013 to April 2019 (red bar).

5. Summary and Conclusions

A series of on-site topographic and bathymetric surveys were conducted along a 20 km long stretch of shoreline from north of the Wushi Fishery Port to the south of the Lanyang River estuary in June 2006, April and September 2012, April and September 2013, and April and October 2019. A total of 43 planned survey track lines designed for sonar collection were spaced approximately 500 m apart in the alongshore direction. Each track line was of varying length to allow the maximum water depth to reach 10–15 m (deeper than the closure depth), and topographic and bathymetric surveys were completed in 2 days. The bathymetric data obtained from several on-site surveys and the collected 0 m isobaths in various years were employed to investigate the long-term erosion and accretion along the studied shoreline. The 0 m isobath evolution reveals that the construction of a jetty and groin for the Wushi Fishery Port caused erosion and accretion to occur to the north and south, respectively. The interannual comparisons of the alongshore and cross-shore profiles indicate that dramatic erosion occurred in the southern Lanyang River estuary from 2013 to 2019 due to the establishment of a nature reserve. However, slight accretion occurred from 2013 to 2019 in the northern Lanyang River estuary because the riverine sediments were carried northward by tidal currents. In winter, the strong northeast monsoon induced sustained large waves, and the shortage of riverine sediment supply led to erosion of the coastal areas of northeastern Taiwan. In contrast to winter, weaker waves and large amounts of sediment released from the river (because of high river discharge) in summer were beneficial for accretion in the coastal areas of northeastern Taiwan. The cross-profile evolutions indicate that the supply of riverine sediment in the southern Lanyang River estuary was reduced in the past two decades as a result of the gradual northward movement of the Lanyang River mouth. The shoreline affected by estuarine sediment is approximately 2 km long from north to south of the Lanyang River alongshore. Long-term alongshore erosion and accretion are natural processes in coastal areas; however, the loss of coastal lands could be a result of overexploitation, e.g., the designs and constructions of the fishery

port and backwater for the coastal areas. Although the present study provides insight into the problems of management and development for the coastal environment, more frequent topographic and bathymetric surveys for the whole shoreline of Taiwan should be conducted in the future. Additionally, numerical simulations are necessary for future research to explain the seasonal mechanism of the simulations of the seasonal and annual change for wavefield, tidal current, and alongshore sediment transport.

Author Contributions: Conceptualization, T.-Y.L., S.-C.H., C.-H.C., T.-Y.C., W.-B.C., W.-P.H., W.-D.G., J.-Y.H. and C.-H.L.; on-site surveys, T.-Y.L., C.-H.C., T.-Y.C., W.-B.C., W.-P.H., W.-D.G., J.-Y.H. and C.-H.L.; data collection and analysis, T.-Y.L., C.-H.C., T.-Y.C., W.-P.H. and W.-B.C.; writing—original draft preparation, W.-B.C. and S.-C.H.; writing—review and editing, W.-B.C. and S.-C.H. All authors have read and agreed to the published version of the manuscript.

Funding: This research was supported by the National Science and Technology Center for Disaster (NCDR), Ministry of Science and Technology (MOST), Taiwan.

Institutional Review Board Statement: Not applicable.

Informed Consent Statement: Not applicable.

Data Availability Statement: Publicly available datasets were analyzed in the present study. The data can be found here: <https://ocean.cwb.gov.tw/V2/> (accessed on 5 January 2022).

Acknowledgments: The authors would like to thank the Central Weather Bureau and the Water Resource Agency, Taiwan, for providing the measurements of waves and currents.

Conflicts of Interest: The authors declare no conflict of interest.

References

- Rueda, A.; Vitousek, S.; Camus, P.; Tomás, A.; Espejo, A.; Losada, I.J.; Barnard, P.L.; Erikson, L.H.; Ruggiero, P.; Reguero, B.G.; et al. A global classification of coastal flood hazard climates associated with large-scale oceanographic forcing. *Sci. Rep.* **2017**, *7*, 5038. [CrossRef] [PubMed]
- Mentaschi, L.; Vousdoukas, M.I.; Pekel, J.-F.; Voukouvalas, E.; Feyen, L. Global long-term observations of coastal erosion and accretion. *Sci. Rep.* **2018**, *8*, 12876. [CrossRef] [PubMed]
- Pang, J.Z.; Si, S.H. Evolution of the Yellow River mouth: I. Historical shifts. *Oceanol. Limnol. Sin.* **1979**, *10*, 136–141.
- Pang, J.Z.; Jiang, M.X.; Li, F.L. Changes and development trend of runoff, sediment discharge and coastline of the Yellow River Estuary. *Trans. Oceanol. Limnol.* **2000**, *4*, 3–6.
- Wright, L.D.; Wiseman, W.J.; Bornhold, B.D.; Prior, D.B.; Suhayda, J.N.; Keller, G.H.; Yang, Z.S.; Fan, Y.B. Marine dispersal and deposition of Yellow River silts by gravity-driven underflows. *Nature* **1988**, *332*, 629–632. [CrossRef]
- Blodgett, H.W.; Taylor, P.T.; Roark, J.H. Shoreline changes along the Rosetta-Nile Promontory monitoring with satellite observations. *Mar. Geol.* **1991**, *99*, 67–77. [CrossRef]
- Frihy, O.E.; Komar, P.D. Long-term shoreline changes and the concentration of heavy minerals in beach sands of the Nile Delta, Egypt. *Mar. Geol.* **1993**, *115*, 253–261. [CrossRef]
- Huang, H.J.; Li, C.Z.; Guo, J.J. Application of Landsat images to the studies of the shoreline changes of the Huanghe River Delta. *Mar. Geol. Quat. Geol.* **1994**, *14*, 29–37.
- Huang, H.J.; Wang, Z.Y.; Zhang, R.S. The error analysis of the methods of monitoring the beach changes using digital photogrammetry, satellite images and GIS. *Mar. Sci.* **2002**, *26*, 8–10.
- Ji, Z.W.; Hu, C.H.; Zeng, Q.H. Analysis of recent evolution of the Yellow River Estuary by Landsat images. *J. Sediment. Res.* **1994**, *3*, 12–22.
- Xue, C.T. Historical changes in the Yellow River Delta, China. *Mar. Geol.* **1993**, *113*, 321–329. [CrossRef]
- Xue, C.T. Division and recognition of modern Yellow River Delta lobes. *Geogr. Res.* **1994**, *13*, 59–66.
- Sun, X.G.; Yang, Z.S. Prediction of modern Huanghe River Delta area increment by using the sediment discharge. *Oceanol. Limnol. Sin.* **1995**, *26*, 76–82.
- Li, G.X.; Wei, H.L.; Han, Y.S.; Cheng, Y.J. Sedimentation in the Yellow River Delta: Part I. Flow and suspended sediment structure in the upper distributary and the estuary. *Mar. Geol.* **1998**, *149*, 93–111. [CrossRef]
- Li, F.L.; Pang, J.Z.; Jiang, M.X. Shoreline changes of the Yellow River Delta and its environmental geology effect. *Mar. Geol. Quat. Geol.* **2000**, *20*, 17–21. (In Chinese)
- White, K.; Asmar, H.M. Monitoring changing position of coastlines using Thematic Mapper imagery, an example from the Nile Delta. *Geomorphology* **1999**, *29*, 93–105. [CrossRef]
- Dias, J.M.A.; Boski, T.; Rodrigues, A.; Magalhaes, F. Coastline evolution in Portugal since the Last Glacial Maximum until present—A synthesis. *Mar. Geol.* **2000**, *170*, 177–186. [CrossRef]

18. Xu, J.X. A study of thresholds of runoff and sediment for the land accretion of the Yellow River Delta. *Geogr. Res.* **2002**, *21*, 163–170.
19. Yu, L.S. The Huanghe (Yellow) River: A review of its development, characteristics, and future management issues. *Cont. Shelf Res.* **2002**, *22*, 389–403. [[CrossRef](#)]
20. Chang, J.; Liu, G.H.; Liu, Q.S. Analysis on spatio-temporal feature of coastline change in the Yellow River Estuary and its relation with runoff and sand-transportation. *Geogr. Res.* **2004**, *23*, 339–346.
21. Syvitski, J.P.M.; Vorosmarty, C.J.; Kettner, A.J.; Green, P. Impact of humans on the flux of terrestrial sediment to the global coastal ocean. *Science* **2005**, *308*, 376–380. [[CrossRef](#)] [[PubMed](#)]
22. Murray, N.J.; Phinn, S.R.; DeWitt, M.; Ferrari, R.; Johnston, R.; Lyons, M.B.; Clinton, N.; Thau, D.; Fuller, R.A. The global distribution and trajectory of tidal flats. *Nature* **2019**, *565*, 222–225. [[CrossRef](#)] [[PubMed](#)]
23. Chen, W.-B.; Liu, W.-C.; Hsu, M.-H.; Hwang, C.-C. Modelling investigation of suspended sediment transport in a tidal estuary using a three-dimensional model. *Appl. Math. Model.* **2015**, *39*, 2570–2586. [[CrossRef](#)]
24. Nienhuis, J.H.; Ashton, A.D.; Edmonds, D.A.; Hoitink, A.J.F.; Kettner, A.J.; Rowland, J.C.; Törnqvist, T.E. Global-scale human impact on delta morphology has led to net land area gain. *Nature* **2020**, *577*, 514–518. [[CrossRef](#)]
25. Dunn, F.; Darby, S.; Nicholls, R.; Cohen, S.; Zarfl, C.; Fekete, B. Projections of declining fluvial sediment delivery to major deltas worldwide in response to climate change and anthropogenic stress. *Environ. Res. Lett.* **2019**, *14*, 1–11. [[CrossRef](#)]
26. Warrick, J.A.; Stevens, A.W.; Miller, I.M.; Harrison, S.R.; Ritchie, A.C.; Gelfenbaum, G. World’s largest dam removal reverses coastal erosion. *Sci. Rep.* **2019**, *9*, 13968. [[CrossRef](#)] [[PubMed](#)]
27. Hapke, C.J.; Kratzmann, M.G.; Himmelstoss, E.A. Geomorphic and human influence on large-scale coastal change. *Geomorphology* **2013**, *199*, 160–170. [[CrossRef](#)]
28. Angamuthu, B.; Darby, S.E.; Nicholls, R.J. Impacts of natural and human drivers on the multi-decadal morphological evolution of tidally-influenced deltas. *Proc. R. Soc. A* **2018**, *474*, 20180396. [[CrossRef](#)] [[PubMed](#)]
29. Hurst, M.D.; Rood, D.H.; Ellis, M.A.; Anderson, R.S.; Dornbusch, U. Recent acceleration in coastal cliff retreat rates on the south coast of Great Britain. *Proc. Natl. Acad. Sci. USA* **2016**, *113*, 13336–13341. [[CrossRef](#)] [[PubMed](#)]
30. Dadson, S.; Hovius, N.; Chen, H.; Dade, W.B.; Hsieh, M.-L.; Willett, S.D.; Hu, J.-C.; Horng, M.-J.; Chen, M.-C.; Stark, C.P.; et al. Links between erosion, runoff variability and seismicity in the Taiwan orogen. *Nature* **2003**, *426*, 648–651. [[CrossRef](#)] [[PubMed](#)]
31. United Nations International Strategy for Disaster Reduction (UNISDR). In *Global Survey of Early Warning Systems: An Assessment of Capacities, Gaps and Opportunities towards Building a Comprehensive Global Early Warning System for All Natural Hazards*; United Nations International Strategy for Disaster Reduction: Geneva, Switzerland, 2006.
32. Leaman, C.K.; Harley, M.D.; Splinter, K.D.; Thran, M.C.; Kinsela, M.A.; Turner, I.L. A storm hazard matrix combining coastal flooding and beach erosion. *Coast. Eng.* **2021**, *170*, 104001. [[CrossRef](#)]
33. Romagnoli, C.; Sistilli, F.; Cantelli, L.; Aguzzi, M.; De Nigris, N.; Morelli, M.; Gaeta, M.G.; Archetti, R. Beach Monitoring and Morphological Response in the Presence of Coastal Defense Strategies at Riccione (Italy). *J. Mar. Sci. Eng.* **2021**, *9*, 851. [[CrossRef](#)]
34. Shih, H.-J.; Chen, H.; Liang, T.-Y.; Fu, H.-S.; Chang, C.-H.; Chen, W.-B.; Su, W.-R.; Lin, L.-Y. Generating potential risk maps for typhoon-induced waves along the coast of Taiwan. *Ocean Eng.* **2018**, *163*, 1–14. [[CrossRef](#)]
35. Chang, C.-H.; Shih, H.-J.; Chen, W.-B.; Su, W.-R.; Lin, L.-Y.; Yu, Y.-C.; Jang, J.-H. Hazard Assessment of Typhoon-Driven Storm Waves in the Nearshore Waters of Taiwan. *Water* **2018**, *10*, 926. [[CrossRef](#)]
36. Houston, J.R. Simplified Dean’s method for beach-fill design. *J. Waterw. Port Coast. Div.* **1996**, *122*, 143–146. [[CrossRef](#)]
37. Hanson, H.; Kraus, N.C. Long-Term Evolution of a Long-Term Evolution Model. *J. Coast. Res.* **2011**, *SI 59*, 118–129. [[CrossRef](#)]
38. Frey, A.E.; Connell, K.J.; Hanson, H.; Larson, M.; Thomas, R.C.; Munger, S.; Zundel, A. *GenCade Version 1 Model Theory and User’s Guide*; Technical Report ERDC/CHL TR-12-25; U.S. Army Engineer Research and Development Center: Vicksburg, MS, USA, 2012.
39. Medellín, G.; Torres-Freyermuth, A.; Tomasicchio, G.R.; Francone, A.; Tereszkievicz, P.A.; Lusito, L.; Palemón-Arcos, L.; López, J. Field and Numerical Study of Resistance and Resilience on a Sea Breeze Dominated Beach in Yucatan (Mexico). *Water* **2018**, *10*, 1806. [[CrossRef](#)]
40. Puleo, J.A.; Cristaudo, D.; Torres-Freyermuth, A.; Masselink, G.; Shi, F. The role of alongshore flows on inner surf and swash zone hydrodynamics on a dissipative beach. *Cont. Shelf Res.* **2020**, *201*, 104134. [[CrossRef](#)]